

Microstructure and Mechanical Properties of Pulse Laser Welded Stainless Steel and Aluminum Alloys for Lithium-Ion Cell Casings

Vallabha Rao Rikka¹, Sumit Ranjan Sahu¹, Rajappa Tadepalli¹, Ravi Bathe², Thyagarajan Mohan¹, Raju Prakash¹, Gade Padmanabham² and Raghavan Gopalan^{1*}

1. Centre for Automotive Energy Materials, International Advanced Research Center for Powder Metallurgy and New Materials (ARCI), Taramani, Chennai 600113, India

2. Centre for Laser Processing of Materials, International Advanced Research Center for Powder Metallurgy and New Materials (ARCI), Balapur, Hyderabad 500005, India

Abstract: Similar joining of highly thermal conductive and optical reflective aluminum alloy Al 3003 and SS alloy SS316 for hermetic sealing of lithium-ion cell casing application has been investigated using Nd:YAG pulsed laser welding. Microstructural investigations were carried out to characterize the welding zone interface by optical microscopy and scanning electron microscopy. Industrial X-ray 3D computed tomography was carried out on the welding zone to identify the defects such as spatters, gas voids, recast and tapers. It was found that spatters exist in weld zone of SS316L lid and case and show higher hardness (HV 200-210) in the weld area compared to the base metal (HV-175-10) due to fine-grained microstructure. In the case of Al 3003, the laser welding parameters were optimized to obtain 100% joint efficiency with defect free weld zone, and the hardness behavior was dictated by grain size and annealing effects. Furthermore, the welded casings of the cylindrical cells of Li-ion battery were subjected to He-leak detection to ascertain the hermiticity.

Key words: Laser welding, lithium-ion batteries, aluminum alloys, hardness, microstructure, X-ray 3D computed tomography, He-leak detection.

1. Introduction

Lithium-ion (Li-ion) batteries have emerged as the most promising power sources for electric vehicles/hybrid electric vehicles (EVs/HEVs) due to their high energy density, high specific power and long cycle life [1-3]. Li-ion cell fabrication process involves the assembly of various components. Electrodes (cathode and anode) are fabricated using current-collector foils (Al and Cu) and are wound together followed by injection of electrolyte to build the electrochemical system. Due to the reactive nature of the electrolyte and other cell components, the

Li-ion cell components have to be closed in a hermetically sealed casing (or can/container) after assembly.

Cell casing materials are typically made up of stainless steel, nickel-plated mild steel, aluminum and its alloys. Several factors such as mechanical properties and casing material weight determine the applicability of casing materials for hermetic sealing. The energy density of the battery in EVs is dictated by the total weight, including casings. Aluminum, due to its lower density, is preferred as a light-weight choice for EV batteries [4]. However, for long term operation under harsh conditions and safety requirement, stainless steel is more suitable material for battery casing, due to its excellent performance in crash energy management, higher strength and excellent

*Corresponding author: Raghavan Gopalan, associate director, research fields: high Tc superconductors, magnetic materials, Li-ion battery, thermoelectric and structure-property correlation of functional materials.

For welding experiments, 150 mm × 100 mm sized specimens were cut and edges of the plates were polished to minimize the gaps between the joint surfaces. To remove oxide layer and residuals from the surface of the samples prior to welding, wire brushing was done, followed by acetone wash. In addition, representative cylindrical battery casings of SS 316L (33 mm diameter × 60 mm height × 1 mm thick) and Al 3003 (33 mm diameter × 60 mm height × 2 mm thick) were welded (lid to case) using the laser parameters mentioned in Table 2.

Pulsed Nd:YAG laser (1,064 nm wavelength) was used for welding the plates without filler material. The laser beam was focused on the samples by a specially built optical system consisting of a beam expanding telescope (BET) and a lens of 80 mm focal length, giving a beam diameter 600 μm at the focal point. The focal plane of the laser was positioned at the surface of the sheet. Argon shielding gas was fed through a 4 mm diameter nozzle in the trailing mode configuration at a gauge pressure of 2 bar, 18 L/min flow rate at a nozzle standoff distance of 3 mm. Initially bead-on-plate welds were carried out to optimize the weld parameters for laser welding of 0.5 mm thick SS 316L, 1 mm thick Al 3003 and 2 mm thick Al 3003 plates.

The plates were held in place using a fixture and argon gas was used as shielding during both the SS 316L and Al3003 alloys welding to protect the melt from oxidation. The k-type thermocouple was used to

measure the temperature of the cylindrical casing at a distance ~5 mm away from the joint during welding. After welding, the plates were visually observed for gross defects. Samples for microscopy and hardness measurements were sectioned in the direction perpendicular to the welding direction. Specimens were then mounted, polished and etched. An optical microscope coupled with image analyzer was used to first observe the weld microstructures and make measurements of the weld profile. Detailed microscopic and elemental analyses were performed using a scanning electron microscope (SEM) equipped with energy dispersive X-ray spectroscopy (EDS).

Vickers micro-hardness tests were performed on the cross-sectional specimens across the weld zone, heat-affected zone (HAZ) and base material with a load of 200 gf for SS 316L and 50 gf for Al 3003 with a spacing of 150 μm between subsequent indents. Hermeticity of the cylindrical casings welded using optimized parameters in Table 2, were checked by He-leak detection system. A tube of 8 mm diameter was welded to the lid and a vacuum pump was connected to the cylindrical casing through the tube and evacuated completely. This setup was linked to the helium mass spectrometer (leak detector). The pressurized helium gas was sprayed along the weld seam (joint) to check the hermeticity of the weld zone. To investigate the depth of penetration and defects existing in the weld zone, high resolution industrial X-ray 3D computed tomography was conducted on the weld casings.

Table 2 Optimized laser welding processing parameters for Al 3003 and SS 316L plates.

Sample	Pulse width (ms)	Rep rate (Hz)	Pulse energy (J)	Process speed (mm/s)	Sheet thickness(mm)
SS 316L	10	20	11	7	0.5
Al 3003 (Specimen 1)	8	10	42	4.2	2
Al 3003 (Specimen 2)	5	30	20	8.4	1
Al 3003 (Specimen 3)	5	12	20	3	1
Al 3003 (Specimen 4)	5	12	20	4	1
Al 3003 (Specimen 5)	5	12	20	4	1

3. Results and Discussion

3.1 Microstructure

Scanning electron micrographs (SEM) of the SS 316L weld cross-section are shown in Fig. 2 with clearly identified fusion zone, heat affected zone (HAZ) and base metal microstructures (Fig. 2a). The microstructure of fusion zone consists of fine cellular grains resulting from the localized heating and consequence rapid solidification inherent to the pulsed laser welding process. The HAZ shows columnar grain growth almost perpendicular to the solid-liquid boundary. It has been fairly well established in the welding literature that the microstructures of the fusion zone and the HAZ are determined by the temperature gradient at the solid-liquid interface G and the growth rate R , during the solidification of an alloy [8, 9]. The ratio G/R determines the mode of solidification (planar, cellular, dendritic, columnar or equiaxed), while the product $G \times R$ represents the cooling rate that affects the size of the microstructure [10]. The fine-grained microstructure observed in the fusion zone is a result of high cooling rates, which are

typically seen in the laser welding process (Fig. 2b). The solidification mode in the fusion zone is in the planar-cellular regime, owing to a relatively high G/R ratio due to laser welding [11]. Large thermal gradients also resulted in the growth of columnar grains almost perpendicular to the boundary of the fusion line (Fig. 2c).

SS 316L welds exhibit a tensile strength of 551 ± 51 MPa and maximum elongation of $24 \pm 10\%$ compared to 580 MPa and 49% respectively for the base material. Effectively the joint efficiency is about 95% for laser welding of SS 316L plates. Fracture occurred at the fusion zone-HAZ interface. The type and size of the microstructures have been shown to determine the tensile properties [12, 13]. With a relatively well-defined HAZ, it is likely that discontinuities such as precipitates form at the grain boundaries leading to a slight weakening of the joint.

Al welding is more challenging compared to SS welding since Al has higher thermal conductivity and a high reflectivity of the laser beam. Therefore, Al welding typically needs higher power that has to be supplied at a faster rate compared to SS welding [4, 14].

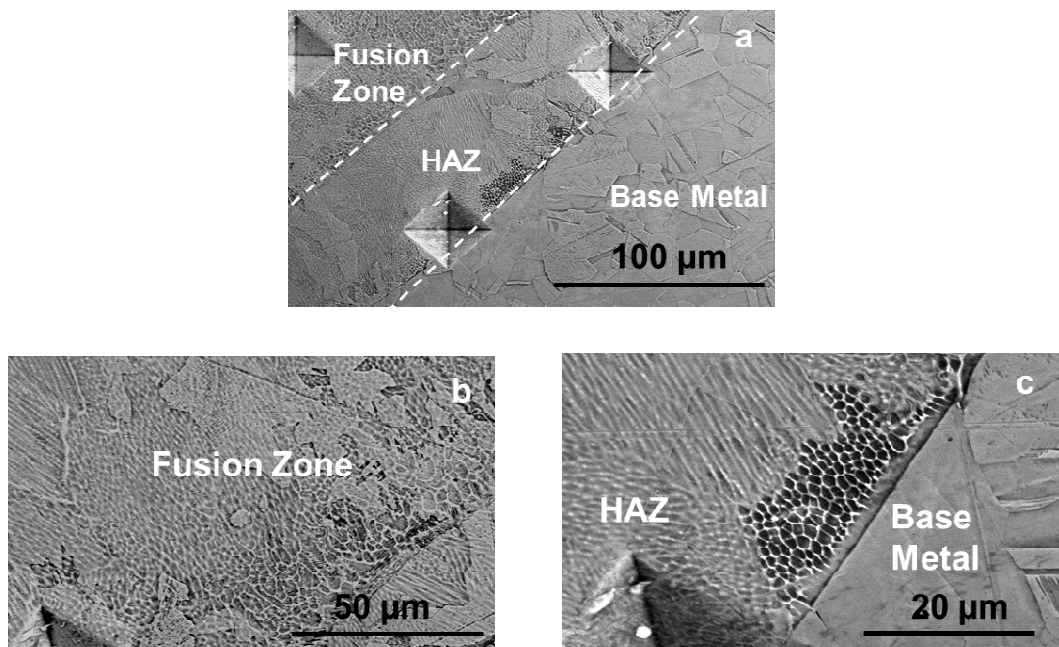


Fig. 2 Cross-sectional SEM micrographs of laser welded 0.5 mm thick SS 316L plates: (a) welding zone showing fusion zone, HAZ and base metal microstructures, (b) magnified view of fusion zone and (c) magnified view of HAZ-base metal interface.

The process parameters for welding of 2 mm thick Al 3003 plates are detailed in Table 2. As such, higher pulse energy (42 J for 2 mm sheets) was needed to achieve full penetration welds. Process instability and spatter was observed during welding of Al 3003 with short pulse duration and high pulse energy parameters. It was also observed that welding at lower speed resulted in the formation of undercut and underbead. The welding without Argon inner blanket resulted in the formation of pores/micro-cracks due to oxidation. The visual surface quality of Al 3003 welds were acceptable for the parameters listed in Table 2. The parameters have sufficient high power density to produce a sufficient key-hole to enable full penetration of the laser beam into the Al 3003 alloy.

3.2 Mechanical Properties

Figs. 3a and 3c show the hardness profiles of 0.5 mm and 2 mm thick welded SS 316L and Al 3003 sheets, respectively. Figs. 3b and 3d shows optical image of corresponding weld cross-sections along

with the indentation profiles from Vickers micro-hardness tests. Both graphs show a similar trend of hardness, with a harder fusion zone compared to the base metal.

For SS 316L, it can be observed that the hardness shows a steady increase from the base metal (HV 175-180) to the fusion zone with a plateau of HV 200 – 210 in the fusion zone. The hardness of the HAZ is in between these two zones. The hardness profile follows a typical microstructure-dependent pattern. Fine-grained microstructure in the fusion zone results in higher hardness while the HAZ has intermediate hardness corresponding to the columnar microstructure. Whereas, the laser welded zone of Al 3003 shows a very fine-grained structure with no clear distinction between the fusion zone and HAZ, indicating a very narrow HAZ. The hardness behavior of laser welded Al 3003 shows a distinct softness in the HAZ (HV 40-43) and an increase in hardness in the fusion zone (HV 54-58). While the fusion zone hardness is higher is due to the fine-grained structure

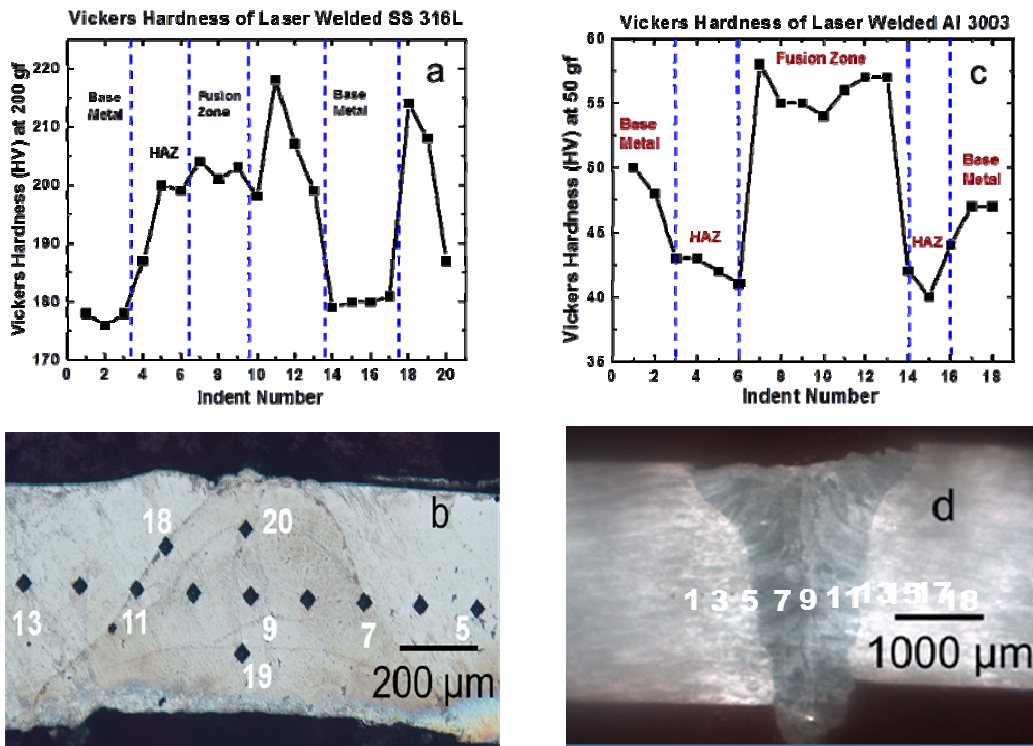


Fig. 3 Micro-hardness profiles across the weld area and cross-sectional micrographs of laser welded plates. (a, b) 0.5 mm thick SS316L plate, (c, d) 2 mm thick Al3003 plate.

(as in the case of SS 316L), the hardness drop in the HAZ is related to the nature of Al 3003 alloy. Al 3003 is a non-heat treatable alloy which is strengthened by strain hardening. It shows that the laser welding process caused an annealing effect in the HAZ that caused a reversal of the strain hardening effect. Consequently, the hardness in this zone dropped below that of the base material.

Tensile tests of welded 2 mm and 1 mm thick Al 3003 sheets were carried out. The base materials show different strength for the 2 mm and 1 mm sheets (189 vs. 93 MPa), which is possibly due to different temper of the two materials. The 2 mm thick sheets were of “H14” temper, while the 1 mm thick sheets were of “O” temper. The joint efficiency is 100% or higher for the 1mm thick sheets and ~70% of the 2 mm thick sheets. It is interesting to note that the specimens # 1 and 2 failed at the fusion zone-HAZ interface which is weakened due to annealing effects from the welding process. This weakening resulted in a lower strength compared to the base material. In contrast, specimens # 3-5 failed at the HAZ-base metal interface. In this case, the strength is equal or greater compared to that of the base material. Welding of non heat-treatable alloys produces a HAZ with the mechanical properties

of an annealed “O” temper alloy and such behavior is validated in this study. 1 mm samples showed largely ductile fracture in both base metal and weld zone whereas 2 mm samples showed both ductile and brittle fracture in base metal and weld zone (Figs. 4b, 4c, 4e and 4f). Gross defects were found in the samples. Tensile test of 0.5 mm SS 316L sample was also carried out. Ultimate tensile strength (UTS) of the weld zone was 95% of that of base metal. No gross defects were found in this case. Base metal showed dimple ductile fracture and weld zone showed some flat facets (Figs. 4a and 4d).

3.3 He-Leak Test and X-Ray 3D Tomography

He-leak test and high resolution X-ray 3D computed tomography were carried out to ascertain the quality and hermeticity of the welded cylindrical casing of the Lithium ion cells. 1 mm diameter tube was inserted and welded to the lid for injecting the He gas. The lid attached to the tube was welded to the casing as shown in Fig. 5 for both SS316L and Al3003 using the optimized parameters (Table 2). The maximum temperature in the casing during the welding process was found to be < 60 °C, which is within the safety range (< 80 °C) to prevent battery

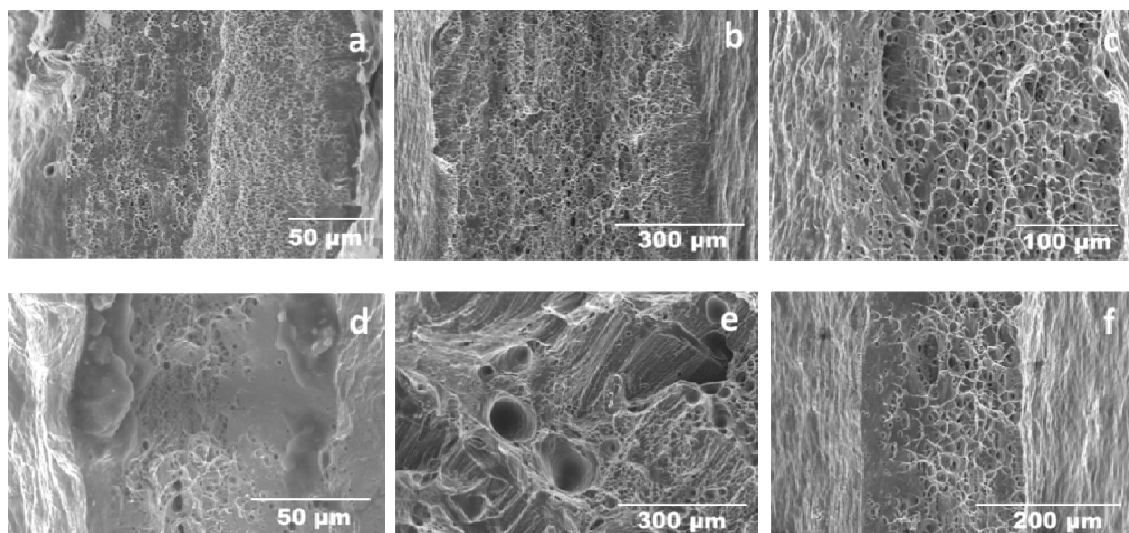


Fig. 4 SEM fractograph of (a) 0.5 mm SS 316L base metal, (b) 2 mm Al 3003 base metal, (c) 1 mm Al 3003 base metal, (d) weld zone for 0.5 mm SS 316L specimen, (e) weld zone for 2 mm Al 3003 specimen and (f) weld zone for 1 mm Al 3003 specimen.

material degradation [7]. He-leak tests of SS 316L and Al 3003 welded cylindrical casings showed no leak with a limit of $< 4.4 \times 10^{-9}$ mbar-L/s.

X-ray 3D computed tomography scan was conducted on laser welded SS 316L and Al 3003 cylindrical battery casings to ascertain the quality of the welding. It was found that the welding was obtained with utmost hermeticity for both SS 316L and Al 3003 casing sealing. Figs. 5a and 5f are the X-ray tomography 3D view of the welded SS 316L and Al 3003 cylindrical casings respectively. Figs. 5b-5d show images taken from 2.12, 2.43 and 2.49 mm depth from the weld surface of SS 316L casing (measured using scene coordinate systems) and Figs. 5g-5i) are from depth of 3.75, 2.85 and 0.13 mm from the weld surface of Al 3003 casing. The welding

penetration depth was measured by finding the difference of values from the z-coordinate. For SS316L case sealing the welding depth was approximately 0.37 mm while it was 3.62 mm for Al 3003 cell. In case of SS 316L welding, randomly distributed spatters were observed in the sealing zone at a welding depth of 2.43 mm (Fig. 6a) where in the case of Al 3003 there were no spatters throughout the welding depth (Fig. 6b). The formation of spatters observed in SS 316L during welding probably due to high power density

Overall, both SS 316L and Al 3003 were found to be acceptable candidate materials for battery casings which can be welded by pulse laser. Al is preferred over SS, due to its low density, especially when we look for automotive applications where the battery

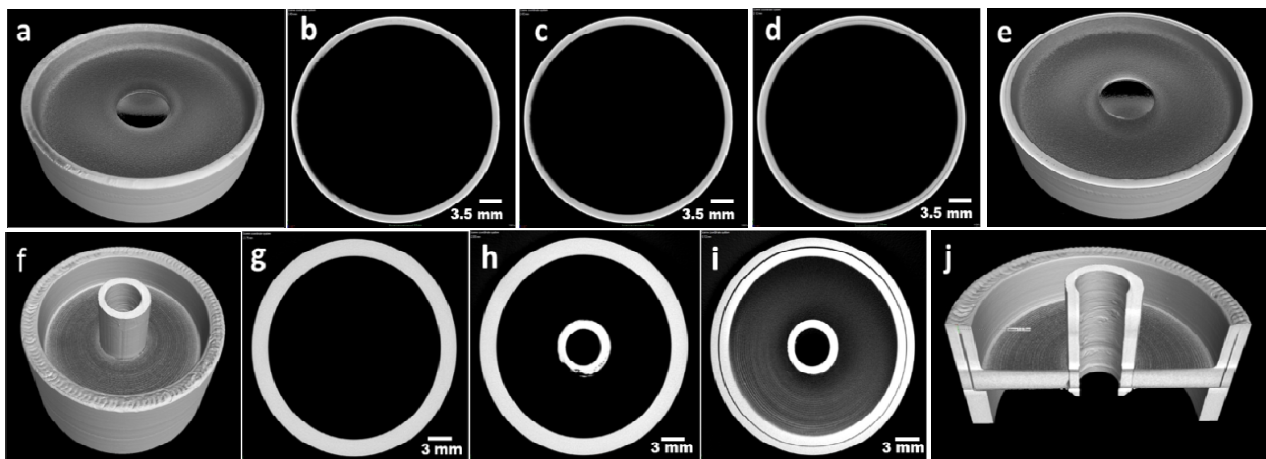


Fig. 5 (a-e) X-ray 3D-computed tomography cross section images of SS 316L cylindrical cell, (f-j) Al 3003 cylindrical cell taken at various depth of weld zone from surface.

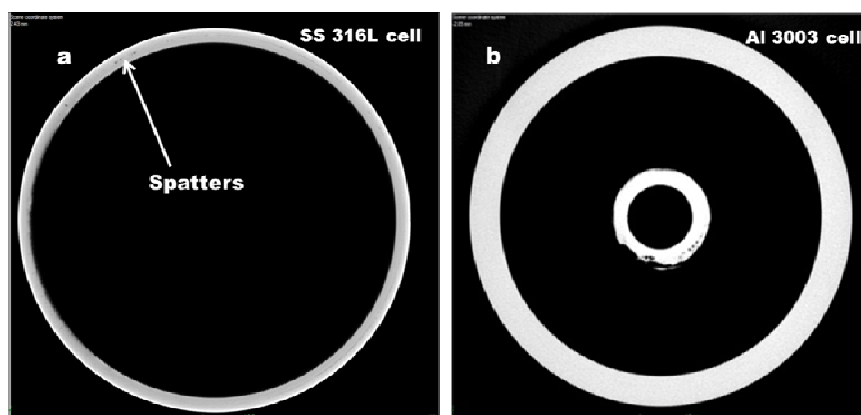


Fig. 6 (a) SS 316L weld zone with spatters, (b) Al 3003 weld zone without spatters.

pack needs to be as light as possible. Further investigations on the specific tests for the use of laser welded casings for battery applications, such as pressure testing, corrosion, are in progress.

4. Conclusions

In summary, Nd:YAG laser welding characteristics of SS 316L and Al 3003 for Li-ion battery casing application were investigated. Weld parameters were optimized for butt welding of 0.5mm thick SS 316L and 2mm thick Al 3003 plates. SS 316L weld zone and HAZ showed higher hardness than the base material due to fine-grained microstructure. The joint efficiency for SS 316L welds was found to be about 95%. Al 3003 welds showed a softening behavior in the HAZ due to relaxation of strain hardening and increased hardness in the fusion zone due to small grain size. The joint efficiency for Al 3003 welds was nearly 100% which has resulted in an efficient welding. Hermetic sealing of battery casings was confirmed using He-leak detection tests and X-ray 3D computed tomography.

Acknowledgments

We thank Prof. G. Sundararajan (DES, ARCI) for support and suggestions. We thank Prof. Krishnan Balasubramanian (Department of Mechanical engineering, IITM Chennai) for conducting high resolution X-ray 3D computed tomography. We are grateful to the Department of Science & Technology, Government of India, for supporting this work under the project 'Development of Li-ion batteries for EV application (IR/S3/EU/0001/2011).

References

- [1] Scrosati, B. and Garche, J. 2010 "Lithium Batteries: Status, Prospects and Future." *Journal of Power Sources* 195: 2419-30.
- [2] Armand, M. and Tarascon, J. M. 2008. "Building Better Batteries." *Nature* 451: 652-7.
- [3] Kang, B. and Ceder, G. 2009. "Battery Materials for Ultrafast Charging and Discharging." *Nature* 458: 190-3.
- [4] Narukawa, S., Amazutsumi, T., Fukuda, H., Itou, K., Tamaki, H. and Yamauchi, Y. 1998. "Development of Prismatic Lithium-Ion Cells Using Aluminum Alloy Casing." *Journal of Power Sources* 76: 186-9.
- [5] Choi, D., Wang, W. and Yang, Z. 2011. *Material Challenges and Perspectives*. Yuan X, Liu, H. and Zhang, J. (eds), CRC Press, 1-50.
- [6] Chu, J. 2013. "Crash-Testing Lithium-Ion Batteries." Massachusetts Institute of Technology. Accessed January 16, 2017. <http://phys.org/news/2013-06-crash-testing-lithium-ion-batteries.html>.
- [7] Vetter, J., Novak, P., Wagner, M. R., Veit, C., Moller, K.-C. and Besenhard, J. O. *et al.* 2005. "Ageing Mechanisms in Lithium-Ion Batteries." *Journal of Power Sources* 147: 269-81.
- [8] Chowdhury, S. M., Chen., D. L., Bhole, S. D., Powidajko, E., Weckman, D. C. and Zhou, Y. 2011. "Microstructure and Mechanical Properties of Fiber-Laser-Welded and Diode-Laser-Welded AZ31 Magnesium Alloy." *Metallurgical and Materials Transactions A* 42: 1974-89.
- [9] Ventrella, V. A., Berretta, J. R. and De Rossi, W. 2010. "Pulsed Nd:YAG Laser Seam Welding of AISI 316L Stainless Steel Thin Foils." *Journal of Materials Processing Technology* 210: 1838-43.
- [10] Kou, S. 1987. *Welding Metallurgy*. New York.
- [11] Molian, P. A. 1985. "Solidification Behaviour of Laser Welded Stainless Steel." *Journal of Materials Science Letters* 4: 281-3.
- [12] P'ng, D. and Molian, P. 2008. "Q-Switch Nd:YAG Laser Welding of AISI 304 Stainless Steel Foils." *Materials Science and Engineering A* 486: 680-5.
- [13] Quan, Y. J., Chen, Z. H., Gong, X. S. and Yu, Z. H. 2008. "Effects of Heat Input on Microstructure and Tensile Properties of Laser Welded Magnesium Alloy AZ31." *Materials Characterization* 59: 1491-7.
- [14] Nerádová, M. and Kovačócy, P. 2010. "Welding of Aluminum Using a Pulsed Nd:YAG Laser." *Acta Polytechnica* 50: 66-9.